

Natural Element Method: a new trade-off between FEM and meshfree methods?

Abstract — This paper is mainly focused on the Natural Element Method. Based on a Voronoï cell diagram, new shape functions are introduced and used to solve Maxwell equations with both Galerkin or point collocation approaches. The computational performance is illustrated through several examples, and compared to results provided by classic Finite Element Method and also by Element-Free Galerkin method.

I. Introduction

Mesh-based computational simulation methods are largely used in analysis and modeling of physical phenomena in engineering. Nowadays a traditional method, such as the Finite Element Method (FEM), relies on a high level of development. The experience in the investigation of a wide range of problems and the availability of many commercial software packages are undeniable advantages of this method [1].

Although its well-established capabilities, its narrow dependency on a mesh structure brings some limitations that become progressively apparent as the simulation requirements become more sophisticated. The mesh-based approximation in classic FEM is not suited for the treatment of local effects like eddy currents and discontinuities that do not coincide with elements edges. The accuracy of the method is closely related to the regularity of the elements as well. In consequence, in problems that involve displacements, for instance, the distortion of elements can degrade results. Remeshing strategy can be used in order to keep a good mesh quality, although this process is costly and technically complex, especially in 3D. Moreover, the “mapping” of the field quantities between the successive meshes is also a costly process that usually leads to degradation of accuracy [1].

In the 90s some alternative numerical methods have started drawing more attention of the computational simulation community. The general goal has been to overcome the limitations related to the narrow mesh-dependency. Some of these alternatives can be regarded as improvements of traditional approaches and some others are based upon relatively new concepts, such as a total independency of a mesh structure – at least for the interpolation of the field variable.

The Element-Free Galerkin method (EFG) [2] and the Natural Element Method (NEM) [3] are two major examples of these new approaches developed over the last years. While the first doesn't make use of any mesh at all for the solution approximation construction, the latter uses a discretization scheme based on *Voronoi cells* as support. If both of them overcome in a good measure the referred limitations of the classic Finite Element Method, the NEM is a more recent method that has not been as explored as the EFG by the simulation community.

This work is concentrated on the Natural Element Methods, addressing the description and analysis of its main concepts and characteristics. A series of benchmarking problems is presented, where the NEM performance is compared to the

FEM, EFG and analytical solutions.

The article structure is organized as follows:

The [section II](#) presents a summary of the main developments in terms of alternatives to the classic finite element method.

A brief overview of the element-free Galerkin method is presented in the [section III](#). Some particular concepts associated to the class of methods frequently referred as *meshless methods* are introduced.

The Voronoï diagrams/cells and related concepts are developed in [section IV](#). The construction of specific shape functions based on Voronoï diagrams and their application in both collocation and Galerkin techniques are described.

The [section V](#) focuses the treatment of the boundary and interface conditions in the NEM and the coupling with the FEM.

The [section VI](#) addresses the Natural Finite Difference Method (NFD), a finite difference scheme on irregular grids based on the natural neighbor concept.

In the [section VII](#), performance of the NEM and NFD on the resolution of some benchmarking problems is showed. The error is computed through dual formulations or analytical reference. Results are compared to FEM and EFG.

[Section VIII](#) presents the application of the NEM in a series of realistic problems, covering low and high frequency applications. A FEM-coupled simulation of an electrical machine is also presented.

The general analysis of the obtained results and the perspectives about further research on the Natural Element Method are presented in the [section IX](#).

Technical works that were basis for this article are referenced in the [section X](#).

II. Alternatives to FEM: from meshless to natural neighbors methods

The classification of the several approaches that emerged mainly over the last two decades is somewhat controversial. On the whole, they are frequently referred as *meshless* or *meshfree* methods, even for the case of the techniques that use some kind of space discretization but are not rigidly restricted by it.

Ideally, meshless or meshfree methods are numerical simulation techniques in which no mesh is necessary at all throughout the process of solving a physical problem [1]. In general, the basic idea is using a *cloud of nodes* to represent the problem domain and its boundaries. Any *a priori* information about connectivity between nodes is needed. The function approximation is made entirely in terms of nodal data. In such conditions, the improvement of the solution in specific regions is done simply by adding nodes and the treatment of problems involving large displacements can be done more robustly [4]. However, in general the computational cost of the solving process in meshless methods tends to be higher than in FEM. This issue will be addressed in

the next section for the specific case of the EFG method, but it can be roughly generalized.

In practice, some of the methods claimed as meshless are not “truly meshless”. Methods based upon the Galerkin procedure generally make use of a background mesh or integration grid for the integration of the matrices derived from the weak form. However, one can say that the mesh used in the integration procedure is not necessarily restricted by the details constraints of the problem geometry, being much simpler to generate. Moreover, the field quantities interpolation is still independent of any mesh structure. Further discussion about this issue will be carried out throughout this work.

Hereafter we present a brief summary of some of the main developments in the so called meshless methods. More extensive and detailed overview works covering the principal methods can be found in [1],[4-9].

The concept of mesh independency was introduced by Lucy [10] and Gingold and Monaghan [11] with the Smoothed Particle Hydrodynamics (SPH) in 1977. This point collocation particle method is based on the kernel estimates approximation and its direct goal was to solve unbounded astrophysics problems. Until the 90s the research on the application of the SPH method in other classes of problems than astrophysics was very modest, with some works addressing its application in fluid dynamics. In the 90s the method started to be applied in solid mechanics and a series of improvements were incorporated into SPH, since the original version suffered from spurious instabilities and inconsistencies [9]. The Reproducing Kernel Particle Method (RKPM), introduced by Liu et al. in 1995 [24] is an example of improvement in the SPH concepts. It has both Galerkin and point collocation versions.

Other point collocation methods emerged in the 90s, using several approximation techniques, such as *least square* (LSQ), *weighted least square* (WLS), *radial basis functions* (RBF), etc. [5].

Another branch of the so called meshless family had its starting point with the work of Nayroles et al. in 1991, developing the Diffuse Elements Method (DEM) [12]. This method makes use of the *moving least square* (MLS) local interpolation over a cloud of nodes and a Galerkin procedure. The DEM was the first meshless method to be applied in electromagnetic problems, in 1992, by Maréchal et al. [13]. In 1994 Belytschko et al. proposed some improvements in the DEM, developing the Element-Free Galerkin method (EFG) [2]. Since its introduction in the computational simulation community, the EFG has been one of the most explored meshless methods, with several application works and improvements. Being methods based on a global weak form and the Galerkin technique, both DEM and EFG make use of the background mesh for integration purposes.

In attempt to eliminate the integration grid or background mesh, the Meshless Petrov-Galerkin method (MLPG) was introduced by Atluri and Zhu in 1998 [14]. This method makes use of the concept of *local weak form*, which allows the background mesh to be created in sub-domains. Although the concept of background mesh still exists, this method is said to be essentially a meshless method because the creation of the background mesh in this case is much simpler than the *global weak form* methods – as the DEM and EFG method, for instance – once the integrations are performed over overlapping and regularly shaped sub-domains.

Originally, the MLS approximation scheme was used in the MLPG method, but later variations of the method were developed with the use of different approximation schemes, such as radial basis functions, Shepard function, RKPM, etc. [15].

One of the evident drawbacks of using the classic MLS interpolation is that this scheme does not present the Kronecker delta function property. Hence the imposition of boundary conditions commonly requires the implementation of some additional technique, such as Lagrange Multipliers, penalty methods, coupled finite element, etc. [7].

Aiming to replace MLS functions, Liu and Gu proposed the Point Interpolation Method (PIM) in 1999 [16]. This method uses polynomial interpolation technique, leading to excellent accuracy and shape functions that possess the Kronecker delta function property. In our community, this method is deeply studied and developed by Mesquita and his group [36]. The initial versions of the method presented some limitations related to the singularity of the moment matrix and the numerical stability [1]. However the method has been continuously improved and applied to a large range of problems. This method has been applied to both Galerkin and local Petrov-Galerkin formulations.

The *partition of unity* concept [18] was used as basis for the construction of a series of new approaches. Some of them were presented as FEM extensions. In these cases, the basic principle is to use the partition of unity concept to enrich locally the solution based on *a priori* knowledge about the function being approximated. It allows the solution to reproduce special characteristics like discontinuities and singularities without the costly requirements of mesh refinement and/or remeshing of the classic FEM. Some examples of these methods are the Partition of Unity Finite Element Method (PUFEM), presented by Melenk and Babuska in 1996 [19], and the Extended Finite Element Method (XFEM), presented by Belytschko et al. in 1999 [20,21].

The h-p Clouds method is another example of partition of unity based method. It was presented by Duarte and Oden in 1995 [17]. The h-p stands for the possibility of adaptivity in *h* and *p*. The method's fundamental idea is the use of the partition of unity concept for the construction of a hierarchical basis [7].

In general, collocation methods and finite differences method using irregular grids present the advantage of not requiring integration at all and, consequently, they can eliminate completely the mesh concept, being truly meshless methods. However, these methods are said to be less stable and accurate when compared to the Galerkin methods [1]. In practice, the concept of meshless method started to be more disseminated in the scientific community after the advent of meshless methods based on the Galerkin procedure – even if some sort of mesh is necessary in the process. Actually, nowadays the requirement of an ordinary mesh as support for the search for neighbor nodes and the numerical integration are not considered a major limitation of these methods, once this kind of mesh is not subjected to the same requirements of quality that are present in FEM. The independence of a mesh structure for the field quantities interpolation is the key feature of this kind of methods.

Another important remark about meshless methods in general is that the physical discontinuities (interfaces of different materials) are not treated naturally as in FEM. Therefore the simulation of inhomogeneous medium requires

the implementation of some additional technique [1].

In 1997 Sukumar et al. presented the Natural Element Method (NEM) [3]. Basically, this method relies on the construction of the Voronoï cells over the problem domain and the concept of *natural neighbors* for the construction of shape functions. This method overcomes all major drawbacks of previous meshless methods, while keeping the smooth and highly accurate solutions observed with the latter. The concept of Voronoï cell functions was also applied to the finite difference approach. The resulting method (NFDM) [23] proves its efficiency in terms of computation time and accuracy even on unstructured grids.

In general, these recent approaches have brought a series of promising results. On the other hand, new challenging issues have emerged and research has been carried out in the last years. Today, in comparison with FEM, these methods are still in an early development phase.

III. Element-Free Galerkin Method

The EFG makes use of the MLS interpolation scheme to approximate the solution of a PDE problem through a Galerkin procedure. The problem domain Ω is represented by a set of N nodes with coordinates \mathbf{x}_i ($i = 1, 2, 3 \dots N$). Each node i has a corresponding *influence domain* or *subdomain* Ω_i , which is the region where the node contributes to the approximation [25]. The size of these subdomains can vary accordingly to the nodes distribution and their union must cover the whole problem domain. In 2D the shape of Ω_i is generally circular or rectangular, as illustrated in the Fig. 1.

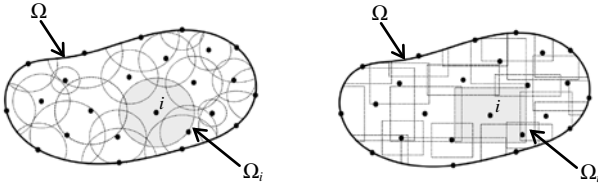


Fig. 1. Clouds of nodes in EFG: left, circular influence domains, right, rectangular influence domains (the influence domains are truncated in the domains borders).

In a real problem, there is much more overlapping between the subdomains than the showed in Fig. 1. It was intentionally decreased in the illustration for sake of clarity.

In the following subsection the procedure for obtaining the shape functions of the classic EFG method in a two dimensions space will be briefly presented.

A. MLS approximation

The MLS approximation is constructed from three components: a *weight function* associated to each node, a *basis* and a set of *coefficients* [25]. The weight function and the basis (generally polynomial) are chosen, while the coefficients are arbitrary unknowns functions of the spatial coordinates $\mathbf{x}^T = [x \ y]$.

Considering a function $u(\mathbf{x})$ defined in the domain Ω , the MLS approximation of this function, denoted by $u^h(\mathbf{x})$, is given by

$$u^h(\mathbf{x}) = \sum_j^m p_j(\mathbf{x}) a_j(\mathbf{x}) \equiv \mathbf{p}^T(\mathbf{x}) \cdot \mathbf{a}(\mathbf{x}) \quad (1)$$

where m is the number of terms in the basis, $p_j(\mathbf{x})$ are

monomial basis functions and $a_j(\mathbf{x})$ are their associated unknown coefficients. Basically, the choice of the basis will be related to the desired consistency order. Common choices are the linear and quadratic bases [6].

The coefficients $a_j(\mathbf{x})$ can be obtained by minimizing the weighted residual J :

$$J = \sum_i^n w_i(\mathbf{x}) \left[\mathbf{p}^T(\mathbf{x}_i) \cdot \mathbf{a}(\mathbf{x}) - u_i \right]^2 \quad (2)$$

where n is the number of nodes whose influence domains cover the point \mathbf{x} , $w_i(\mathbf{x})$ is the value in \mathbf{x} of the weight function associated to the node i and $u_i = u(\mathbf{x}_i)$.

The weight function must be non-zero only over a relative small region around the node, defining its influence domain. This local support feature of the weight function will lead to a banded system matrix. The choice of the weight function is quite free, as long as it satisfies some conditions like positivity, monotonic decreasing and the desired degree of derivability [6]. Examples of weight functions traditionally associated to the EFG method are cubic and quartic splines.

With the minimization of (2) ($\partial J / \partial \mathbf{a} = 0$), the coefficients $a(\mathbf{x})$ can be then calculated in the following form

$$\mathbf{a}(\mathbf{x}) = \mathbf{A}^{-1}(\mathbf{x}) \cdot \mathbf{B}(\mathbf{x}) \cdot \mathbf{U} \quad (3)$$

with the weighted moment matrix \mathbf{A} given by

$$\mathbf{A}(\mathbf{x}) = \sum_i^n w_i(\mathbf{x}) \mathbf{p}(\mathbf{x}_i) \mathbf{p}^T(\mathbf{x}_i), \quad (4)$$

and the \mathbf{B} matrix having the form

$$\mathbf{B}(\mathbf{x}) = [w_1(\mathbf{x}) \mathbf{p}(\mathbf{x}_1) \ \dots \ w_n(\mathbf{x}) \mathbf{p}(\mathbf{x}_n)]. \quad (5)$$

The vector \mathbf{U} collects the function values in the nodes with influence over \mathbf{x} :

$$\mathbf{U} = [u_1 \ \dots \ u_n]. \quad (6)$$

Finally the approximate function can expressed as

$$u^h(\mathbf{x}) = \sum_i^n \phi_i(\mathbf{x}) u_i, \quad (7)$$

where the shape functions are

$$\Phi(\mathbf{x}) = [\phi_1(\mathbf{x}) \ \dots \ \phi_n(\mathbf{x})] = \mathbf{p}^T(\mathbf{x}) \cdot \mathbf{A}^{-1}(\mathbf{x}) \cdot \mathbf{B}(\mathbf{x}) \quad (8)$$

The MLS technique makes the approximated function to be continuous and smooth in the entire problem domain. Major advantages of this technique are the capability of producing an approximation with the desired order of consistency and the possibility of adding enhancements functions that allow the approximate field to model special characteristics such as singularities and discontinuities [1].

One of the drawbacks of this approach is the fact that it generates shape functions that do not possess the Kronecker delta function property (non-interpolating shape functions). It means that the value of the approximation over the nodes is not exactly equal to the actual nodal values. Consequently, the imposition of boundary conditions is not direct.

Another drawback of the method is the need for the moment matrix ($\mathbf{A}_{m \times m}$) inversion for each shape function computation. Besides the computational cost involved in the operation (especially with the use of higher orders basis), there is the possibility of a singular moment matrix as well [9]. Indeed, the moment matrix is invertible when the condition $m \geq n$ is verified. If $m = n$ and the nodes lie on a line, \mathbf{A} will be singular

(if the nodes lie approximately on a line the matrix will be ill-conditioned, yielding inaccurate shape functions values) [26]. This characteristic of the method requires special attention in the nodal topology and the influence domains definition.

In the following subsection, alternatives to overcome some of the classic EFG method drawbacks are described.

B. Interpolating and Improved MLS

The fact that the original MLS scheme is non-interpolating makes the method dependent of the use of special techniques for the imposition of the boundary conditions. Such techniques as, for example, Lagrange Multipliers, penalty method, coupling with FEM, etc., can have disadvantages like the degradation of the system conditioning, the increasing of the number of unknowns, extra computational cost, extra implementation complexity, etc [7].

A straightforward alternative was proposed by Lancaster and Salkauskas [27]. This alternative consists in the use of singular weight functions, like $w_i(\mathbf{x}) = r^{-2t}$, where r is the normalized distance between the node i and the point \mathbf{x} and t a positive integer. The shape functions generated with the use of this kind of weight functions satisfy the Kronecker delta function property, leading to an *Interpolating MLS* scheme. The weight function adopted in this work makes use of a perturbation technique that overcomes some difficulties related to the singularity over the nodes [28]:

$$w_i(r) = \frac{1}{r^{2t} + \varepsilon} \quad (9)$$

where r is the normalized radius (for circular influence domains), given by $r = d_i / d_{mi}$, with d_i corresponding to the distance between \mathbf{x} and \mathbf{x}_i and d_{mi} corresponding to the radius of Ω_i . The parameters t and ε are defined empirically, being $4 \leq t \leq 6$ and $10^{-8} \leq \varepsilon \leq 10^{-12}$ examples of satisfactory ranges for some applications [28]. Difference between the classic and interpolating MLS shape functions is illustrated in Fig. 2.

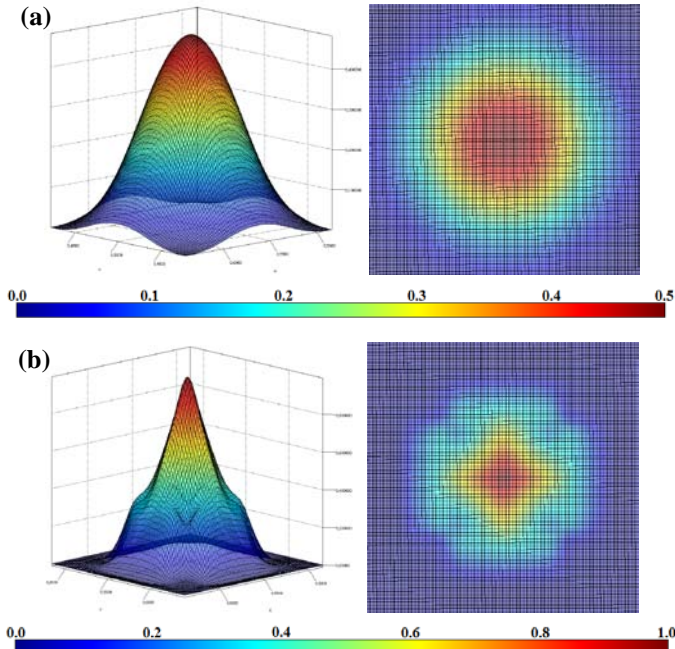


Fig. 2. MLS shape functions: (a) classic shape function using quartic spline weight function; (b) interpolating shape function using (9) with $t = 6$ and $\varepsilon = 10^{-12}$. One can remark in (b) that $\phi_i(\mathbf{x}_i) = 1.0$ and $\phi_i(\mathbf{x}) \approx 0.0$ over the four neighbors nodes.

Another improvement in the method can be done by the use

of orthogonal basis in the MLS approach [29], leading to a scheme commonly referred as *Improved MLS*. The Schmidt orthogonalization procedure can be used to derive an orthogonal basis $\tilde{\mathbf{p}}(\mathbf{x})$, in such way that the following condition is satisfied:

$$A_{kj} = \sum_i^n w_i(\mathbf{x}) \tilde{\mathbf{p}}_k(\mathbf{x}_i) \tilde{\mathbf{p}}_j(\mathbf{x}_i) = 0 \quad \text{for } k \neq j \quad (10)$$

Therefore the moment matrix (4) will have all off-diagonal terms equal to zero and its inverse is calculated directly.

Although this procedure can reduce the computational cost of the moment matrix inversion, the same restrictions relating spatial arrangement of nodes and the conditioning of the moment matrix existing in the classic approach still valid [25].

The EFG code implemented in this work is based on these techniques. The simulations presented were performed using circular influence domains with constant radius and the visibility criterion for the treatment of non-convex boundaries [7].

C. Galerkin procedure

The weak form of the problem is solved through the standard Galerkin procedure. However, typically the integration of the system matrices requires some sort of mesh structure as support for the quadrature points. The common solution of this problem consists in the use of a background mesh as integration support. In this work, for example, a triangular FEM mesh was used. The favorable argument in favor of this approach is that this background mesh can be created without the requisites of mesh quality necessities in FEM, once the shape functions do not use the mesh as support. Indeed, the background mesh is not even necessarily subjected to the problem geometry, being quite easy to implement. In principle, this integration mesh can overpass the domain in a form of a simple rectangular grid, for example, as showed in Fig. 3.

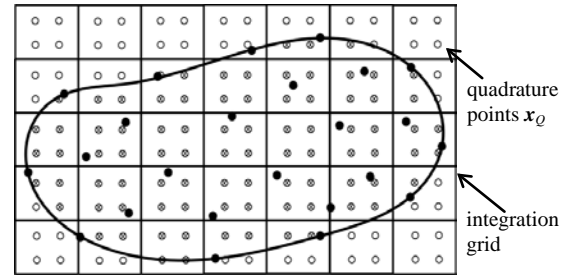


Fig. 3. Integration grid for the hypothetical problem showed in Fig. 1.

Once the background mesh or integration grid is defined, the procedure to evaluate the solution of the PDE problem is quite similar to the standard FEM procedure. The main difference is that the number of nodes that are related to each quadrature point can vary. Actually, each time the expression (8) has to be calculated, a search for the nodes that have influence over \mathbf{x}_Q takes place. In other words, the connectivity between nodes is defined by the superposition of the influence domains and it's determined in run-time. At same time that this feature gives flexibility to the method in the sense of adaptivity and solution refinement, it generates an extra computational cost.

IV. Voronoï Cell Functions

Thanks to this experience on meshless methods, researchers have tried to propose alternatives that keep the good approximation characteristics of the spherical zone of influence around a node, but overcome the intrinsic difficulties mentioned previously such as handling properly physical discontinuities.

In the late 90's, the Natural Element Method (NEM) was proposed [3], based on a Voronoï diagram and Voronoï cells, and the notion of natural neighbors. It provides interpolant shape functions, satisfies partition of unity and linear completeness properties and allows an easy handling of essential boundary conditions, FEM coupling and interfaces between different materials.

This section first introduces Voronoï diagrams and Voronoï cells, then presents Sibson and Laplace shape functions, and last applies these shape functions to solve Maxwell equations with both Galerkin or point collocation approaches.

A. Voronoï Diagram

Let us consider a set of nodes $N = \{n_1, n_2, n_3 \dots n_N\}$ distributed in the whole domain. The Voronoï diagram (1st order Voronoï diagram) is a subdivision of the domain into cells, where each cell C_i associated to node n_i is such that any point in C_i is closer to node n_i than to any other node n_j for $i \neq j$. These cells are the so-called Voronoï cells. In mathematical notation, a Voronoï cell is defined by:

$$C_i = \{\mathbf{x} \in \mathbb{R}^n, d(\mathbf{x}, \mathbf{x}_i) < d(\mathbf{x}, \mathbf{x}_j), \forall j \neq i\} \quad (11)$$

where d is the distance between 2 points in Euclidean metric. Therefore, a Voronoï cell can be seen as the intersection of several half spaces.

Considering for instance a 2D space, C_i is the region of the plane that contains the points closer to node n_i than to any other node as shown in Fig. 4. The Delaunay triangulation, which is the dual of the Voronoï diagram, is built by connecting the nodes that have a common Voronoï facet. Alternatively, the vertices of the Voronoï cell are the center of the circumcircles of the Delaunay triangles. For a given node, its natural neighbors are all the nodes that share a facet of its Voronoï cell. Last, it is also interesting to note that, as opposed to Delaunay triangulation, the Voronoï diagram is unique.

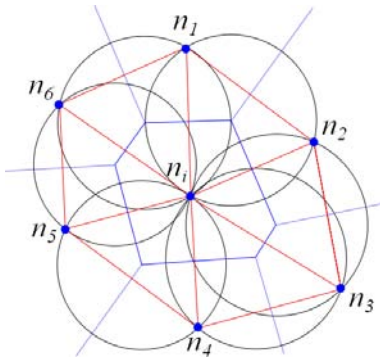


Fig. 4. Voronoï diagram (blue color) and its associated Delaunay triangulation (red color). At node n_i , its Voronoï cell and its 6 natural neighbors n_1 to n_6 .

B. Sibson Natural Shape functions

Data interpolation based on Voronoï cells was initially proposed by Sibson [30] in 1980. For sake of simplicity, we

will consider a set of nodes with known nodal values in a 2D plane, and look for the interpolated value at point \mathbf{x} . The Sibson coordinates Φ_i are measuring the nodes contribution in the interpolation at point \mathbf{x} , in a classical way:

$$u(\mathbf{x}) = \sum_i \Phi_i(\mathbf{x}) \cdot u_i \quad \text{where } u_i \text{ are the nodal values} \quad (12)$$

To build Sibson coordinates, point \mathbf{x} is first added to the original Voronoï diagram, defining a new Voronoï cell around \mathbf{x} . This also defines the natural neighbors of \mathbf{x} i.e. the ‘‘closest nodes’’ that will be actually used for the interpolation at \mathbf{x} . They are the nodes that share a common Voronoï facet with the Voronoï cell around \mathbf{x} .

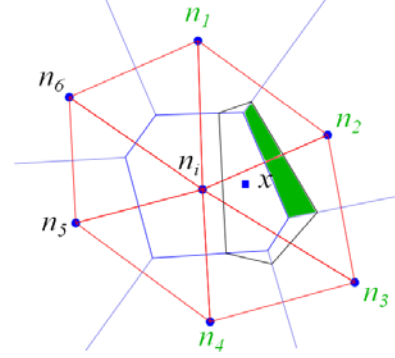


Fig. 5. Sibson natural neighbors and natural coordinates (original Voronoï diagram in blue, natural neighbors in green, additional Voronoï cell due to \mathbf{x} in black, Sibson sub area in green).

The influence of these natural neighbors on the interpolation at point \mathbf{x} is given by (3) where each $A_i(\mathbf{x})$ represents the sub area of the Voronoï cell centered on \mathbf{x} linked to the natural neighbor n_i , as illustrated by the filled region in Fig. 5.

$$\Phi_i(\mathbf{x}) = \frac{A_i(\mathbf{x})}{\sum_j A_j(\mathbf{x})} \quad (13)$$

From (13), it is quite obvious that the natural coordinates are always positive and less than 1, that the sum of all coordinates are equal to 1, and that when \mathbf{x} tends towards n_i , the natural coordinate tends towards 1 for node n_i and towards 0 for all other nodes. Thus, the partition of unity is satisfied.

$$\forall \mathbf{x}, 0 \leq \Phi_i(\mathbf{x}) \leq 1, \quad \Phi_i(\mathbf{x}_j) = \delta_{ij} \quad \text{and} \quad \sum_i \Phi_i(\mathbf{x}) = 1 \quad (14)$$

Since the linear completeness property can also be demonstrated [3], natural coordinates are very much appropriate to serve as shape functions and will be called Sibson shape function from now on.

Starting from the definition of natural neighbors based the ‘‘empty circumcircle criterion’’ on Delaunay triangles, it is easy to understand that the Sibson shape function extension for a node is in fact the union of all circumcircles passing through this node, as plotted on Fig. 6 (a).

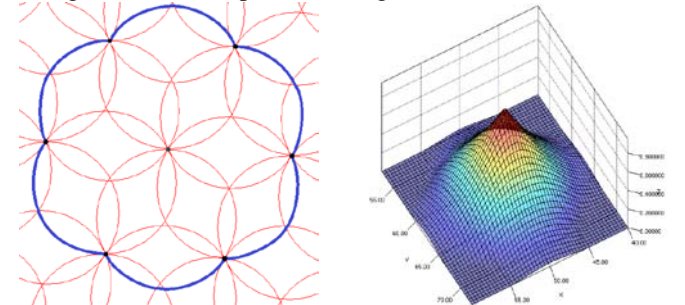


Fig. 6. (a) Support for NEM shape function and (b) Plot of the Sibson shape function.

Last, Fig. 6(b) shows the elevation of the Sibson shape function on a regular grid of nodes. Its smoothness and regularity can be already noticed and will be more thoroughly investigated later.

Extension to n dimensional spaces is immediate. Several works have been proposed using 3D models [31]. It should be noticed however that the complexity of the computation of Sibson shape functions increases significantly in that case.

C. Laplace Natural Shape functions

In the early 2000's, several researchers proposed alternatives to Sibson shape functions, among which the so-called Laplace shape function. This section summarizes the main characteristics and differences of Laplace shape functions with respect to Sibson approach.

On the whole, since Laplace shape functions are based on a Voronoï cell pattern, most the work developed for Sibson shape functions remains valid. In particular the shape function extension is the same, made of the union of the circumcircles containing node n_i . But in 2D (resp. in 3D), Laplace functions are expressed by a ratio of length (resp. surface). Fig. 7 shows the various lengths used in the Laplace shape function expression given in (15).

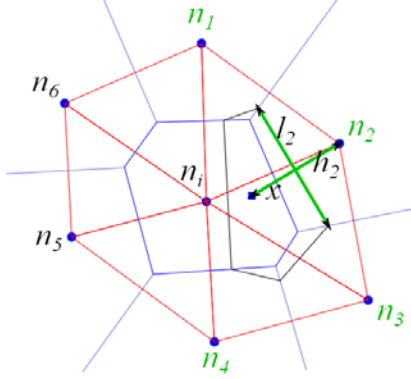


Fig. 7. Laplace NEM shape function computation.

$$\Phi_i(\mathbf{x}) = \frac{\alpha_i(\mathbf{x})}{\sum_j \alpha_j(\mathbf{x})} \quad \text{with } \alpha_i(\mathbf{x}) = \frac{l_i(\mathbf{x})}{h_i(\mathbf{x})} \quad (15)$$

Quite obviously, the partition of unity stands for the same reasons than in the case of Sibson shape functions. Linear completeness of the Laplace interpolation is also valid as shown in [30].

One of the main advantages of Laplace Shape functions is that they involve only length (resp. surface) computation in 2D (resp. 3D) whereas Sibson shape functions need surface (resp. volume) computation in 2D (resp. 3D). More than that, the Laplace shape function has explicit expression for both the shape itself and its derivatives. This is of course a computational advantage when compared to Sibson's functions. On the other hand, continuity property is slightly deteriorated since the Laplace function is C_0 on all edges of circumscribed circles whereas the Sibson's are mostly C_1 except at node location. Fig. 8 shows both functions, the global shapes are of course very similar, but the change in the level of continuity can be noticed.

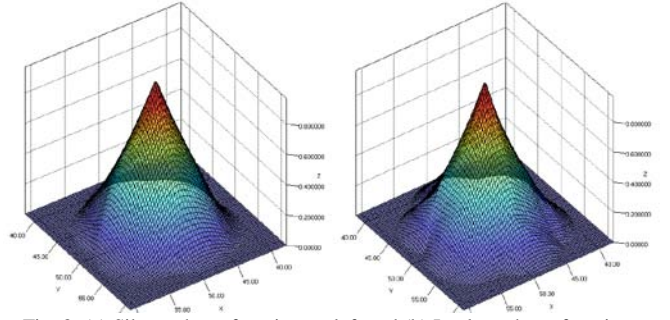


Fig. 8. (a) Sibson shape function on left and (b) Laplace shape function on right.

D. Computation of the shape functions

As one may expect, computation of Voronoï cell shape functions involves many geometric calculation. Considering a given point p , the process consists in:

- Finding out the Delaunay triangles for which the circumcircle enclose point p . The set of external nodes defines the natural neighbors for point p ;
- Insert point p as a new vertex in the triangulation, by deleting interior edges and joining the point p to boundary facets
- Calculate each center of the circumcircles of the new triangulation. These centers are the vertices of the new Voronoï cell related to point p .
- Last, if Laplace (resp. Sibson) shape functions are expected calculate the length of the facets of the Voronoï cell (resp. surface of the 2nd order Voronoï cell).

The following figures depict all this steps.

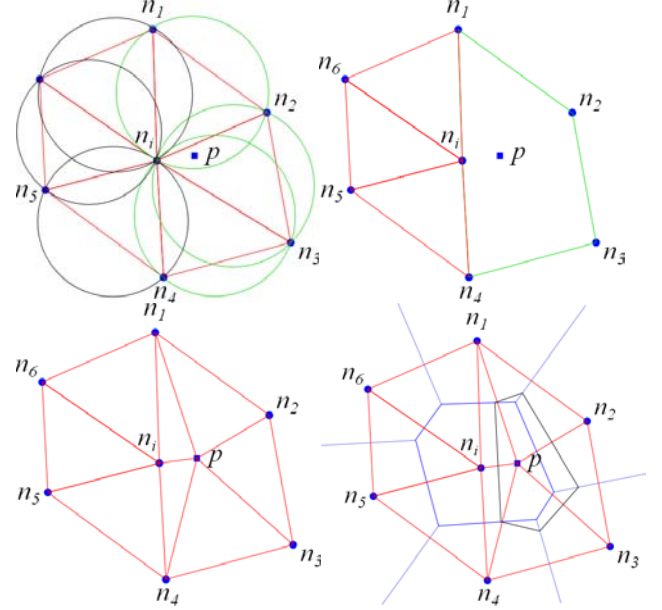


Fig. 9. Shape function calculation procedure at point p .

E. Voronoï cell functions for enhanced post processing

In order to illustrate the efficiency and the relevance of the natural shape functions, we propose to simply post-treat a first order FEM solution using Sibson shape functions. The following figure shows the result obtained on an L shaped capacitance: right, the standard isovalues using FEM interpolation, left the Sibson interpolation of the same nodal values.

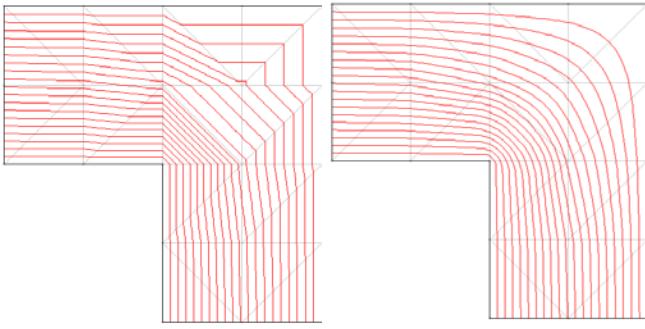


Fig. 10. L shaped capacitance: left, FEM post processing, right, Sibson interpolation of the same nodal values.

The gain in quality is obvious and will be quantified more precisely in section VII.

F. Voronoï cell functions versus FEM or EFG

On one side, when trying to compare FEM with NEM, the analogy with the definition of first order triangular shape function, using barycentric coordinates can of course be underlined.

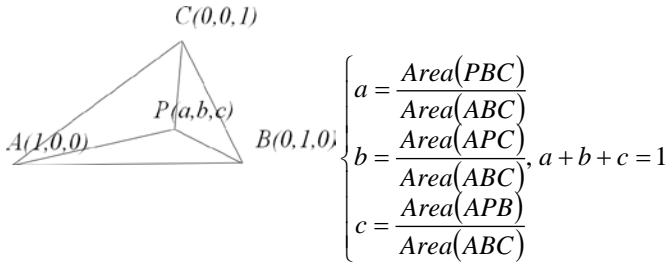


Fig. 11: Barycentric coordinates in a triangle.

The same approach has been used to define Sibson shape functions in (13), and this why the Sibson shape function can also be seen as natural coordinates inside a Voronoï cell.

On the other side, when comparing NEM to EFG, the analogy with meshless approximation is very strong except that instead of having a pure spherical zone of influence around a node, the sphere is pinched at each neighboring nodes to fulfill the interpolation property (see Fig. 6.)

Finally, the following figures summarize the three methods. On the left, FEM interpolation, compared to EFG shape function extension: the regularity of the FEM interpolation is limited and very much oriented by the edges of the elements. On the right, NEM compared to EFG, equivalent regularity and shape function extension, same isotropic interpolation, beyond the edges of the mesh. In that sense, the Natural Element Method belongs to the family of meshless methods, even if for calculation purpose, a triangulation is still used for integration for instance.

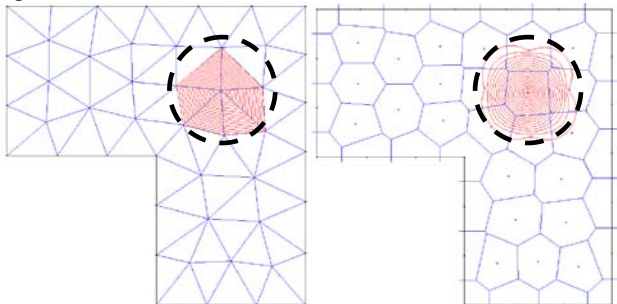


Fig. 12. FME, EFG and NEM shape functions: left, first order FEM compared to EFG shape function extension, right, NEM compared to EFG shape function extension.

V. Natural Element Method for solving Partial Differential Equations

Using either Sibson or Laplace shape functions in a Galerkin procedure is quite straight forward and there is not much to say about it. The main differences with the finite elements implementation are essentially related to code optimization aspects, especially in the integration and assembly parts. Still, some aspects need to be examined in deeper details, namely the boundary and interface conditions, and the ability to couple NEM to FEM.

A. Boundary and interface conditions

On the convex boundary of the study domain, the Voronoï cell based shape functions naturally become linear [3],[31]. Fig. 13 shows the Sibson shape function along an edge of the boundary or on a corner.

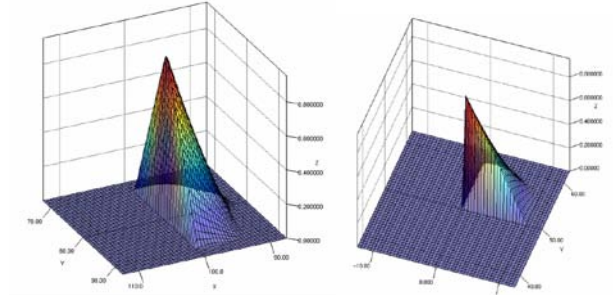


Fig. 13 Representation of the shape function at nodes on the boundary of the domain.

Thus, between two regions with different materials, the continuity of the variable as well as its tangential derivative is ensured, as soon as when interpolating a field in a region, only the nodes of that specific region are considered as natural neighbors (this is exactly what we do when using FEM). This interesting propriety allows the take into account the interface conditions between different materials in a classical weak sense.

Moreover, Voronoï cell functions being interpolant, the essential boundary conditions are also very easy to implement, using the same approach as finite elements.

B. Highly non convex boundaries

For a non-convex boundary and Sibson shape functions, the linear propriety is no more verified. However, since the boundary is usually well discretized, the error made by considering that the Sibson functions are still linear is generally negligible.

It exist some situations where the boundaries are by essence highly non convex, like for instance a crack in non-destructive testing problems.

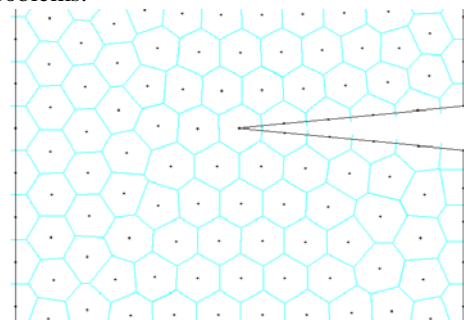


Fig. 14. Non convex boundary and constrained NEM.

In such cases, even if the boundaries are well discretized, the standard Voronoï diagram may consider nodes situated on either side of a crack as natural neighbors, and therefore introduce an undesirable mutual influence.

To overcome this problem, the solution is to use the constrained Delaunay triangulation associated with a criterion of visibility. The constrained Delaunay triangulation allows imposing the edges of the board in the list of edges of the triangulation. The visibility criterion avoids that points on both sides of an internal border become natural neighbors [31].

C. Coupling with the Finite Element Method

Due to its properties, the Natural Element Method can be coupled to finite element method easily contrary to the most of meshless methods. Indeed, the NEM shape functions and the FEM shape functions are the same on the boundaries of a domain. Thus the continuity of the approximation and of the tangential derivatives is naturally ensured.

VI. Voronoï cell Finite difference method

The Voronoï cell can be considered as the elementary cell for the conservation of the divergence of flux at one node. When pushing in that direction, the discrete form of the partial differential equation can be solved using a point collocation scheme. This can be also considered as a finite difference scheme on irregular grids. All the theoretical aspects that are briefly presented below were initially developed by Sukumar [23].

Let us start with a classical magneto-static equation in scalar potential formulation,

$$-\nabla \cdot (\mu (\nabla \Phi)) = 0 \quad (16)$$

and consider the Voronoï cell around node i , Ω_i , as a domain of a region of conservation of the divergence of the flux.

Around each node, using the Gauss theorem, we can write

$$(\nabla \cdot \mathbf{B})_i = \lim_{\Omega_i \rightarrow 0} \frac{\int_{\Omega_i} \nabla \cdot \mathbf{B} \, d\Omega}{\int_{\Omega_i} d\Omega} = \lim_{\Omega_i \rightarrow 0} \frac{\int_{\partial\Omega_i} \mathbf{B} \cdot \mathbf{n} \, d\Omega}{\Omega_i} \quad (17)$$

where Ω_i is the area of the cell around node i . Replacing the flux by its expression in terms of scalar potential, we have:

$$-(\nabla \cdot (\mu \nabla \Phi))_i = \lim_{\Omega_i \rightarrow 0} \frac{1}{\Omega_i} \int_{\partial\Omega_i} \mu \nabla \Phi \cdot \mathbf{n} \, d\Omega \quad (18)$$

Introducing the discrete approximation of Φ , we can further develop the previous equation into:

$$\frac{1}{\Omega_i} \int_{\partial\Omega_i} \mu \nabla \Phi \cdot \mathbf{n} \, d\Omega = \frac{1}{\Omega_i} \sum_j \mu \frac{(\Phi_j - \Phi_i) l_{ij}}{h_{ij}}, \quad \Omega_i = \frac{1}{4} \sum_j l_{ij} h_{ij} \quad (19)$$

where Ω_i is also expressed in terms of l_{ij} and h_{ij} .

Indeed after some several simple manipulations and noticing that $\alpha_{ij} = l_{ij} / h_{ij}$ is part of the Laplace shape function definition, the discrete form of the matrix system of the

magneto-static equation is given by:

$$\begin{cases} \mathbf{K}\Phi = 0 \\ K_{ii} = \sum_j \mu \alpha_{ij} \quad , \quad K_{ij} = -\mu \alpha_{ij} \end{cases} \quad (20)$$

This approach, called from now on Natural Finite Difference Method (NFD), is very interesting since it does not involve any quadrature aspect. It will be tested and compared to FEM and NEM both in terms of accuracy and computation time.

VII. Computational Performances of NEM, FEM and EFG

In this section, we propose to compare computational efficiency - i.e. accuracy for a given cost, of the three numerical methods (NEM, FEM 1st and 2nd orders and EFG). Moreover, a finite difference implementation of Voronoï cell functions (NFD) is also included in the comparison. The aim of this comparison is to locate the NEM in the landscape of numerical methods.

A. Efficiency Results on a Singularity Free test Case

To illustrate the computational performance of each method, we are presenting a first numerical example based on a test problem consisting in a square domain of dimension 1 on each side, where the following equation is solved:

$$\begin{aligned} \Delta u(x, y) &= 2\pi^2 \sin(\pi x) \sin(\pi y) \text{ in } \Omega \\ u(x, y) &= 0 \text{ on } \partial\Omega \end{aligned} \quad (21)$$

The whole domain is initially subdivided into a regular mesh of 32 triangular elements, and is enriched several times by splitting each triangle into 4 new triangles. The analytical solution is given by (2) and allows the calculation of the local error. This problem does not include any singularity and thus, theoretical convergence rates are reachable.

$$u(x, y) = \sin(\pi x) \sin(\pi y) \quad (22)$$

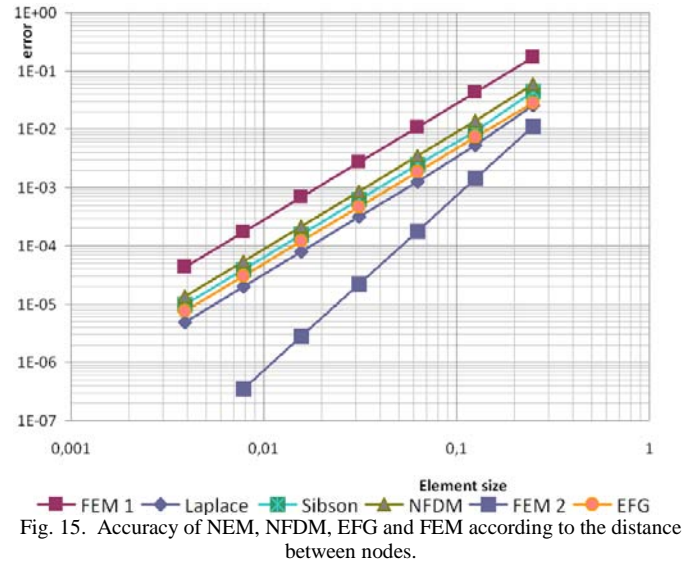


Fig. 15. Accuracy of NEM, NFD, EFG and FEM according to the distance between nodes.

Fig. 15 shows the relative error on the variable, in L^2 norm, computed on the whole domain as the integral of the local error with respect to the mean size of the element edge length. On the whole, NEM and EFG accuracy are globally between the 1st order (FEM1) and the 2nd order FEM (FEM2) accuracies. As expected, both FEM1, EFG and NEM (Laplace,

Sibson or Finite difference) are following a 1st order method slope (h^2) whereas the FEM2 follows a second order (h^3) slope.

Next, Fig. 16 shows that even though the 2nd order FEM is obviously more accurate for a given size of element, all NEM methods are in fact performing better than FEM2 up to 200 degrees of freedom, which is a very interesting result in favor of this interpolation approach. It should be noticed that EFG present the same accuracy as the NEM.

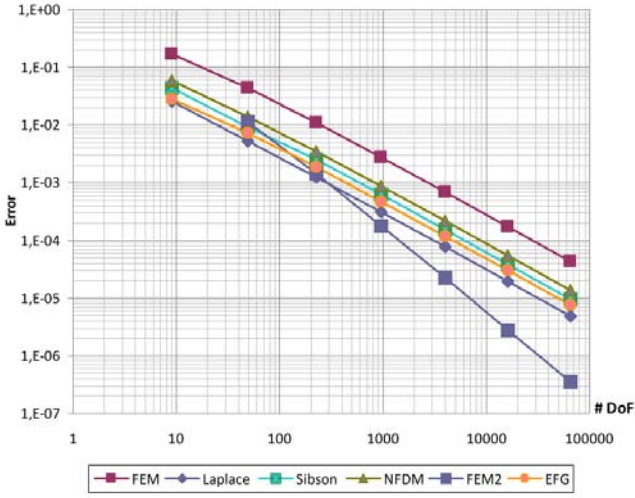


Fig. 16: Error versus the number of degrees of freedom (DoF)

Last, Fig. 17 plots the computational efficiency of all methods, defined as the computational cost for a given accuracy. It clearly shows that for 1st order approximation, NEM is outperforming FEM of nearly 2 orders of magnitude and can even be compared to FEM2 efficiency. But due to a higher convergence rate, superiority of FEM2 increases when the number of degrees of freedom is getting higher. Note that the comparison does not include the EFG method because the code that we have developed for this method is not optimized.

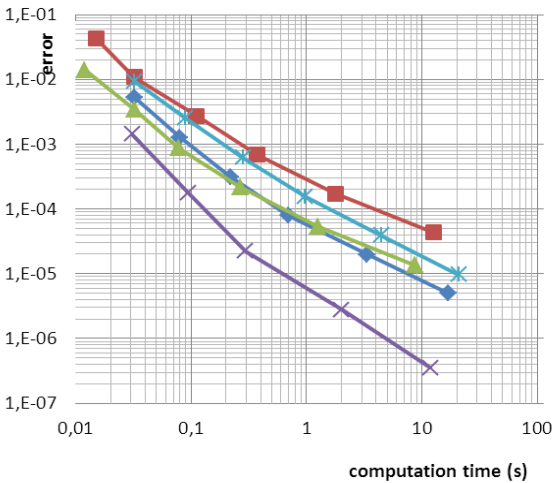


Fig. 17: Computational efficiency of all methods.

To have a better understanding of where the computation time is spent, Fig. 18 plots the time required to build the matrix system (integration and assembly). As expected, due to the large amount of geometric calculation linked to the Voronoï cells, Laplace and Sibson are the most expensive methods. Finite difference Voronoï cell (NFDN) is, to that consideration, much more efficient since no integration and no gradient are required. It is useful to note that numerical integration was carried out using Gauss quadrature approach using 3 Gaussian points.

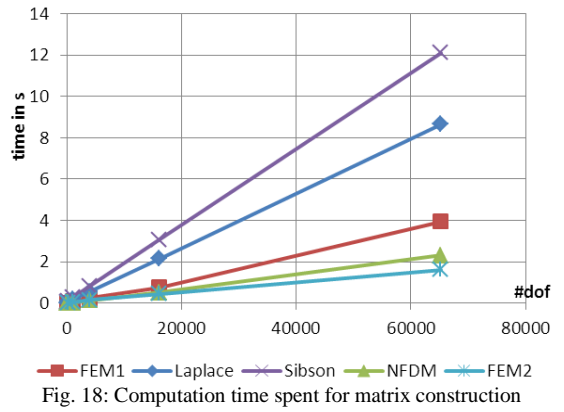


Fig. 18: Computation time spent for matrix construction

Considering the solution solving time, some preliminary considerations must be introduced. First is the band size and second is the condition number. As shown in the table below, the band size is significantly increasing in the case of NEM. This is in fact a direct consequence of its ability to smooth the solution by taking into account information far beyond finite element edges and that property naturally contributes to increase the integration and assembly times for NEM.

TABLE I. BAND SIZE

FEM1	Laplace	Sibson	NFDN	FEM2
7	21	21	9	12

On the other side, the conditioning of the matrix is much better for NEM as Fig. 19 shows. Hence, although the band size is higher, the time spent for the matrix solution calculation with NEM is the cheapest of all methods.

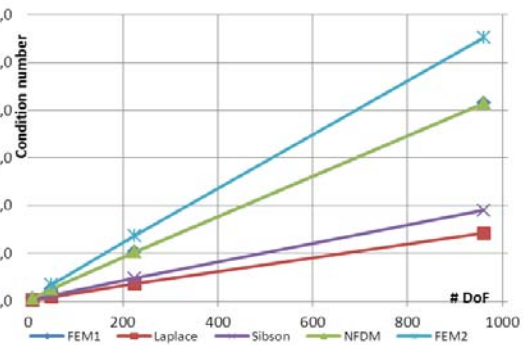


Fig. 19: Condition number of the matrix system for FEM and NEM

B. Efficiency Results on a Test case with Singularity

The second numerical example is based on an electrostatic problem describing an L shaped capacitance. The length of the domain is set to 100 in each direction. Compared to the previous case, this problem includes a singularity at the corner, which will significantly reduce the convergence rate.

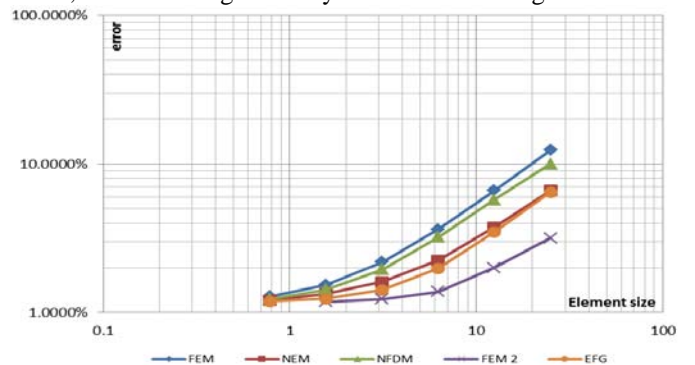


Fig. 20: Accuracy of NEM, NFDN, EFG and FEM according to the distance between nodes for the L shape test case.

Fig. 20 shows that again NEM, NFDM and EFG accuracies are between FEM 1st and 2nd order. Since no analytical solution is available, the error is determined by solving dual formulations. Although for this case, due to the singularity at the corner, accuracy is limited and all methods tend to the same asymptotic behavior. Fig. 21 shows the computational efficiency of all the methods, except EFG. Globally, NEM still outperforms 1st order FEM, and second order FEM behaves even better. But due to the singularity at the corner, accuracy is limited and all methods tend to the same asymptotic behavior.

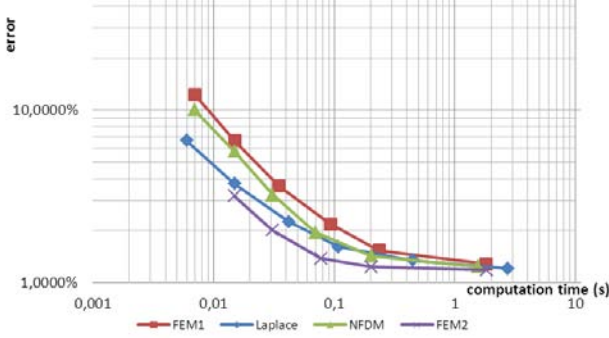


Fig. 21. Computation efficiency for the L shape test case.

VIII. Applications on real world problems

In order to illustrate the relevance and potential of the natural element method to solve different electromagnetic problems, this later is applied to two fields of applications. The first one is an application at low frequency (team workshop 25 and electric machine) and the second one concerns an example at high frequency (electromagnetic scattering problem). In each case, the NEM is compared to FEM.

A. NEM applied to solve magnetostatic problem (Team Workshop 25)

The team workshop 25 is a die model of press with electromagnet for orientation of magnetic powder [32], used for producing permanent magnet. Fig. 22 shows the studied device. It is a 2D magnetostatic non-linear problem.

The weak form of Ampère's law is then given by the classical formulation:

$$R_i = \int_{\Omega} [\mathbf{curl} \mathbf{w}_i \cdot \nu \cdot \mathbf{curl} \mathbf{A} - w_i \mathbf{j}_s \cdot \mathbf{n}] d\Omega = 0 \quad (23)$$

where w_i the shape function and Γ the studied domain. \mathbf{A} and \mathbf{j}_s are the magnetic vector potential and the source current density respectively. Equation (23) leads to a system of nonlinear algebraic equations that can be solved by means of the Newton-Raphson method.

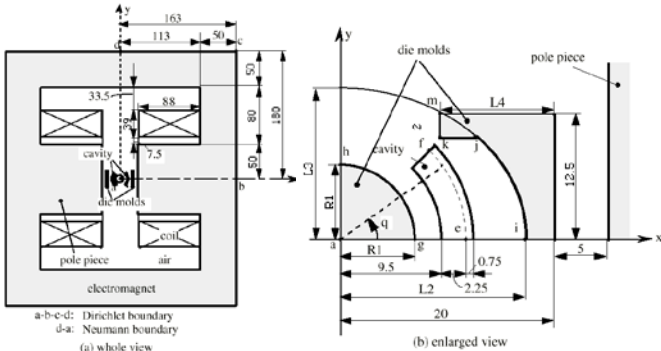


Fig. 22. Model of die press with electromagnet

The problem is solved with NEM and FEM (1st and 2nd orders). Fig. 23 illustrates the flux lines of the magnetic flux obtained by NEM and FEM resolution. A good agreement between the two methods is observed.

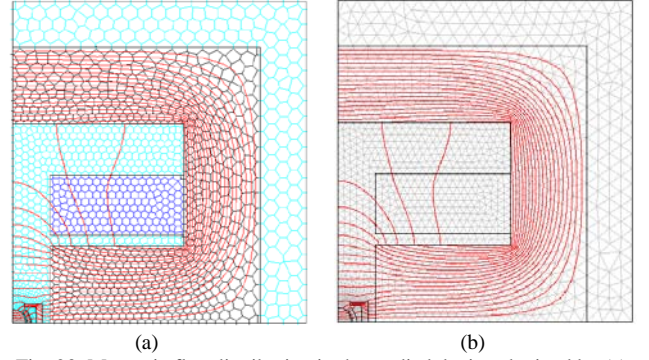


Fig. 23. Magnetic flux distribution in the studied device obtained by (a) nonlinear NEM resolution and (b) non linear FEM resolution.

Fig. 24 plots the computational performance. The reference solution is obtained using a very fine 2nd order FEM solution. On this particular case, the errors are mainly due to the singularities in the corners. It is well known that in such a situation, increasing the number of nodes is much more efficient than increasing the order of approximation. Hence, for a given number of nodes, NEM is more accurate than FEM2, and even if the intrinsic cost of NEM is roughly 3 times more expensive, at the end, both NEM and FEM2 give almost the same computational performance. This tends to clearly demonstrate the very interesting behavior of the Voronoï cell approach: the interpolation has a high degree of continuity.

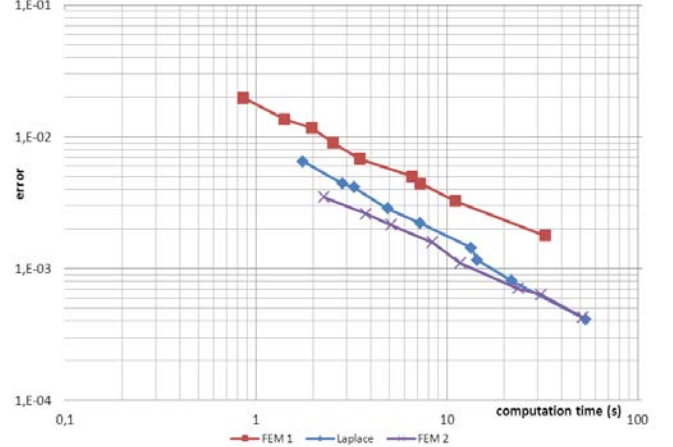


Fig. 24. Computation efficiency for TEAM 25 test case.

B. NEM coupled with FEM to simulate electric machine

Due to its properties, the natural element method can be coupled to finite element method easily contrarily to the most of meshless methods. Indeed, the NEM shape functions are interpolants and become linear at the boundary of the domain. This property shared with FE method allows a natural coupling to the FEM shape functions.

In order to illustrate this interesting property, we have solved the stator of an electric machine using FEM whereas air gap, rotor and bars are solved using the NEM method. Table I. summarizes the main features of the simulated machine. Fig. 25 shows the distribution of the magnetic flux. It has been compared to a pure FEM solution and the both solutions are in good agreement.

TABLE I
THE CHARACTERISTICS OF THE MACHINE

Outer rotor diameter (mm)	108	Inner rotor diameter (mm)	30
Outer stator diameter (mm)	150	Inner stator diameter (mm)	110
Number of phases	3	Stator current density (A/mm ²)	4
Rotor and stator relative permeability	1000	Bar relative permeability	1

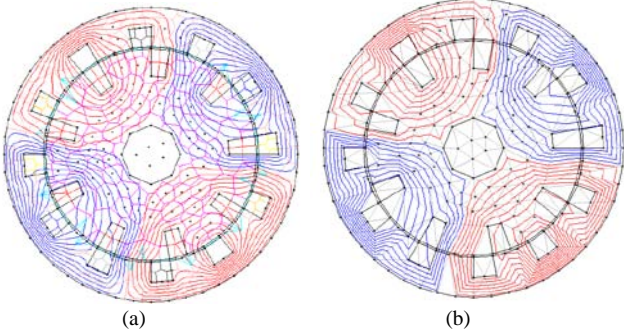


Fig. 25. Magnetic flux distribution in a motor obtained by (a) coupled NEM-FEM resolution and (b) FEM resolution

Coupling FEM and NEM is very interesting in all cases where remeshing is either too complex or leads to unacceptable numerical noise. In this last domain, the ripple torque calculation of motors or numerical derivatives according to geometrical parameters for optimal design according is known to be very sensitive to edge swapping or remeshing. Using NEM in all deformable parts provides an elegant approach to reduce significantly the numerical noise.

C. The Natural Element Method Applied to Solve Electromagnetic Scattering Problem

The numerical solution of the electromagnetic scattering problem is a topic of great interest in sciences and many engineering areas [33]. The Element Free Galerkin Method was already successfully applied to solve arbitrary problems [34]. The aim of this section is to investigate the feasibility and the accuracy of the NEM when applied to study electromagnetic scattering problems. Since the interest is the evaluation of the reliability of the proposed numerical approach and not the analysis of actual cases, the attention is restricted to 2-D problems. To limit the domain, an absorbing boundary condition of first order is applied. Thus, the proposed approach is denominated NEM-ABC. Plane transverse magnetic and electric waves are considered as an excitation. The results are compared with analytical solution and the traditional FEM-ABC method.

Problem formulation

Consider the 2D electromagnetic scattering problem due to non-homogeneous obstacles which properties are uniform along its infinite axis (z-axis) as illustrated in Fig. 26.

For the purpose of analysis, the scattering problem is divided into two regions: Ω_0 , the free space with permeability μ_0 and permittivity ϵ_0 and Ω that may consist in general of non-homogeneous material with permeability $\mu(x,y)$ and permittivity $\epsilon(x,y)$. In this work, both TMz and TEz polarization are considered for the incident electric E_i and magnetic H_i fields and the general expression for them are given by:

$$u_z^i = e^{jk_0(x\cos\theta^i + y\sin\theta^i)} \quad (24)$$

where, $u=Ez$ for TMz or $u = Hz$ for TEz polarization, θ_i is the incident angle shown in the Fig. 26 and $k_0 = \omega \cdot \sqrt{\mu_0\epsilon_0}$ is the wave number.

The Helmholtz differential equation describes the total field behavior in Ω and Ω_0 . The *weak formulation* associated to the wave equation can be written as:

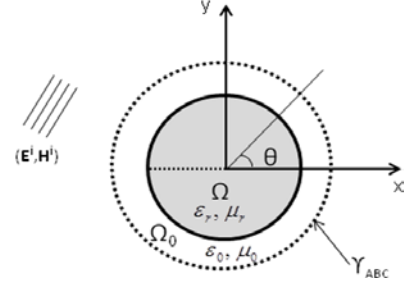


Fig. 26. Arbitrary cylinder illuminated by a plane wave.

$$\int_{\Omega} [\nabla w_i \cdot (\alpha_1 \nabla u) - k_0^2 \alpha_2 w_i \cdot u] d\Omega + \int_{\Gamma_{ABC}} w_i \alpha_1 \frac{\partial u}{\partial n} d\Gamma = 0 \quad (25)$$

where u is an approximation for the electric or magnetic fields and w is the weight function. Also, k_0 represents the wave number, $\alpha_1=1/\mu_r$, $\alpha_2=\epsilon_r$ and $u=Ez$ for electric field polarization, while for magnetic field polarization $\alpha_1=1/\epsilon_r$, $\alpha_2=\mu_r$ and $u=Hz$. To solve this kind of problem by FEM-ABC or NEM-ABC an artificial boundary γ_{ABC} must be chosen beyond the target's border. On the artificial boundary γ_{ABC} , the Wilcox's expansion for the first order of the last term of the right member in (25) gives [35]:

$$\alpha_1 \frac{\partial u}{\partial n} = q - \gamma u \quad (26)$$

In (26) q and γ are given by the following expressions:

$$\gamma = \alpha_1 \left[jk_0 + \frac{\kappa}{2} \right] \quad (27)$$

$$q = \alpha_1 \frac{\partial u^i}{\partial n} + \alpha_1 \left[jk_0 + \frac{\kappa}{2} \right] u^i$$

where κ is the inverse of the distance from the ABC boundary and the center of the target. Now, the final form for the weak formulation could be obtained replacing the last term in (25) by (26) by:

$$\int_{\Omega} [\nabla w \cdot (\alpha_1 \nabla u) - k_0^2 \alpha_2 w \cdot u] d\Omega + \int_{\Gamma_{ABC}} q w d\Gamma + \int_{\Gamma_{ABC}} \gamma w d\Gamma = 0 \quad (28)$$

(28) could be solved by both FEM and NEM methods.

Validation and results

Numerical results for the electromagnetic scattering of various 2D targets are presented in this section. These kinds of problems are typical because many practical scatters as missiles and aircraft fuselage could be represented by 2-D problems. In the first problem, a perfectly conducting cylinder is investigated by a 0.3-GHz TEz plane wave. The second problem considers a semi-open dielectric cavity with $\epsilon_r = 2.56$ and illuminated by a TMz plane wave of 1GHz.

For the first problem, the solution is taken at the half upper cylinders surface for θ ranging from 0° to 180° degrees.

1. Perfectly conducting cylinder

In the first case, the perfectly conducting cylinder of radius 0.3λ is simulated. The studied problem have been discretized in 476 nodes and excited by a TEz plane wave with $\theta_i = 180^\circ$. The external circular boundary, where the ABC of the first order is applied, has radius 0.8λ . The results presented in Fig. 27 shows that the FEM-ABC, the NEM-ABC and the exact solutions are in good agreement. The calculated L^2 norm is 0.09 for FEM-ABC and 0.07 for NEM-ABC. This means that both methods are capable to treat conducting scattering problems.

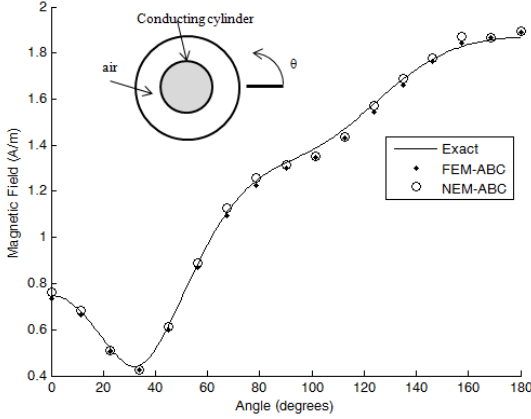


Fig. 27. Absolute value of the total magnetic field over the half upper semicircle of the conductor surface.

2. Dielectric semi-open cavity Dielectric cylinder

In this case a semi-open dielectric cavity is considered. The geometrical parameters of this problem, shown in Fig. 28, are $a = 4\lambda$, $h = \lambda$ and $t = 0.2\lambda$.

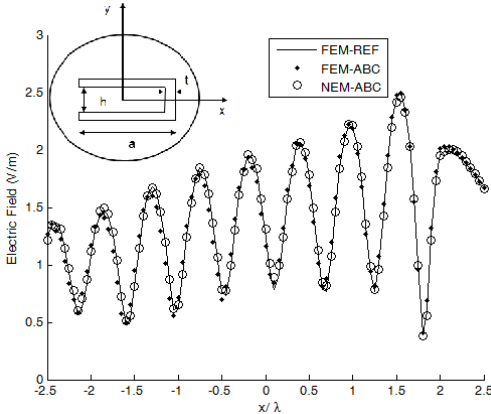


Fig. 28. Absolute value of the total electric field along the x axis

A 1GHz incident TMz wave is assumed to propagate in a direction which lies at an angle of 210° to the axis of the cavity [35]. The cavity dielectric are assumed to have a relative dielectric constant $\epsilon_r = 2.56$. The calculated solutions are compared with the FEM in which a very fine mesh is carried out (Fig. 28 and Fig. 29). A mesh of 7121 nodes is used to compare NEM-ABC and FEM-ABC solutions. The result showed a good concordance between them.

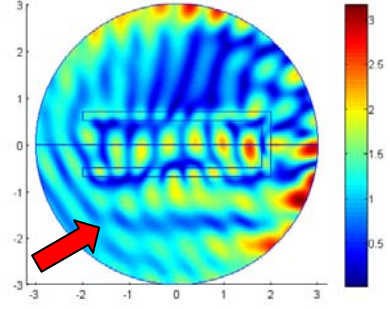


Fig. 29. Iso-values of the electric field magnitude in the semi-open cavity. The arrow represents the direction of the incident field.

IX. Conclusions

In this paper, an overview of main meshless methods is presented. The study is focused on the computational efficiency and the application of the natural element method to 2D electromagnetic problems.

This method can be considered as an interesting alternative to the FEM for several reasons: It presents similar numerical behavior with a better accuracy. It is well adapted to study electromagnetic devices by its property to handle boundary conditions and discontinuities between materials naturally. Last, moving and rotating parts are nicely taken into account since the numerical noise related to edge swapping in the mesh disappears.

In order to deepen the study, the element-free Galerkin meshless method has been also developed and compared to the other methods. The obtained results show that the methods based on Voronoï cell functions – NFDm, NEM – and the EFG method are significantly more accurate than 1st order FEM.

However, it should be noticed that the EFG method present some drawbacks which limit its interest compared to the NEM. Indeed, the definition of the size of the influence domains and the restrictions about the spatial arrangement of nodes can be challenging issues when handling irregular node distributions. Moreover, the search of neighbors requires the use of some additional technique leading to additional computing time. Finally, difficulties are encountered when imposing boundary conditions and treating interfaces discontinuities.

This work has to be extended to higher order NEM shape functions. It will be interesting to perform the same analysis on second order approximation and compare computational efficiency of FEM and NEM in that case. Hopelessly, while higher order approximations were quite easy to produce with EFG, NEM higher approximation is not straightforward. Simulation of 3D problems is also a great challenge.

X. References

- [1] Liu, G. R., *Mesh Free Methods - Moving Beyond the finite Element Method*, USA: CRC Press, 2003.
- [2] Belytschko, T., Liu, Y. Y., and Gu, L., “Element-Free Galerkin Methods,” *International Journal for Numerical Methods in Engineering*, vol. 37, 1994, pp. 229–256.
- [3] Sukumar, N., Moran, B., Belytschko, T., “The Natural Element Method in Solid Mechanics”, *International Journal for Numerical Methods in Engineering*, vol. 43, 1998, pp. 839-887.

- [4] Huerta, A., Rabczuk, T., Belytschko, T., Fernandez-Mendez, S., "Meshfree methods", *Encyclopedia of Computational Mechanics*, Mississauga: John Wiley & Sons, 2004.
- [5] Viana, S. A., Rodger, D., Lai, H. C., "Overview of Meshless Methods", *ICS Newsletter*, vol. 14(2), 2007.
- [6] Belytschko, T., Krongauz, Y., Organ, D., Flemming, M., Krysl, P., "Meshless Methods: An Overview and Recent Development", *Computer Method in Applied Mechanics and Engineering*, vol. 139, 1996, pp. 3-47.
- [7] Li, S., Liu, W. K., *Meshfree Particle Methods*, Berlin: Springer Verlag, 2004.
- [8] Fries, T. P., Matthies, H. G., "Classification and Overview of Meshfree Methods", *Informatikbericht-Nr. 2003-03*, Technische Universität Braunschweig, 2003.
- [9] Nguyen, V. P., Rabczuk, T., Bordas, S. P., Duflo, M., "Meshless methods: A review and computer implementation aspects", *Mathematics and Computers in Simulation*, vol. 79 (3), 2008, pp. 763-813.
- [10] Lucy, B. L., "A Numerical Approach to Testing the Fission Hypothesis," *The Astronomical Journal*, vol. 82 (12), 1977, pp. 1013-1924.
- [11] Gingold, R. A., Monaghan, J. J., "Smoothed Particle Hydrodynamics: theory and application to non-spherical stars", *Monthly Notices of the Royal Astronomical Society*, vol. 181, 1977, pp. 375-389.
- [12] Nayroles, B., Touzot, G., Villon, P., "Generalizing the finite element method: diffuse approximation and diffuse elements", *Computational Mechanics*, vol. 10, 1992, pp. 307-318.
- [13] Maréchal, Y., Coulomb, J. L., Meunier, G., Touzot, G., "Use of the Diffuse Element Method for Electromagnetic Field Computation", *IEEE Transactions on Magnetics*, vol. 29 (2), 1993, pp. 1475-1478.
- [14] Atluri, S. N., Zhu, T., "New Meshless Local Petrov-Galerkin (MLPG) approach in computational mechanics," *Computational Mechanics*, vol. 22 (2), 1998, pp. 117-127.
- [15] Atluri, S., Shengping, S., "The Meshless Local Petrov-Galerkin (MLPG) Method: A Simple & Less-costly Alternative to the Finite Element and Boundary Element Methods", *Computational Mechanics*, vol. 24, 2002, pp. 348-372.
- [16] Liu, G. R., Gu, Y. T., "A point interpolation method for two dimensional solids", *International Journal for Numerical Methods in Engineering*, vol. 50, 2001, pp. 937-951.
- [17] Duarte, C. A., Oden, J. T., "H-p clouds - an h-p meshless method", *Numerical Methods for Partial Differential Equations*, vol. 12 (6), 1996, pp. 673-705.
- [18] Babuska, I., "The partition of unity method", *International Journal for Numerical Methods in Engineering*, vol. 40, 1997, pp. 727-758.
- [19] Melenk, J. M., Babuska, I., "The partition of unity finite element method: Basic theory and applications", *Computer Methods in Applied Mechanics Engineering*, vol. 139, 1996, pp. 289-314.
- [20] Belytschko, T., Black, T., "Elastic crack growth in finite elements with minimal remeshing", *International Journal for Numerical Methods in Engineering*, vol. 45, 1999, pp. 601-620.
- [21] Moes, N., Dolbow, J., Belytschko, T., "A finite element method for crack growth without remeshing", *International Journal for Numerical Methods in Engineering*, vol. 46, 1999, pp. 131-150.
- [22] Sukumar, N., *The Natural Element Method in Solid Mechanics*, PhD dissertation, USA: Northwestern University, 1998.
- [23] Sukumar, N., "Voronoi cell finite difference method for the diffusion operator on arbitrary unstructured grids", *International Journal for Numerical Methods in Engineering*, vol. 57 (1), 2003, pp. 1-34.
- [24] Liu, W. K., Jun, S., Zhang, Y. F., "Reproducing Kernel Particle Methods", *International Journal for Numerical Methods in Fluids*, vol. 20, 1995, pp. 1081-1106.
- [25] Belytschko, T., Dolbow, J., "An Introduction to Programming the Meshless Element Free Galerkin Method", *Archives of Computational Methods in Engineering*, vol. 5 (3), 1998, pp. 207-241.
- [26] Zhuang, X., Augarde, C., "Aspects of the use of orthogonal basis functions in the element-free Galerkin method", *International Journal for Numerical Methods in Engineering*, vol. 81 (3), 2010, pp. 366-380.
- [27] Lancaster, P., Salkauskas, K., "Surfaces generated by moving least squares methods", *Mathematics of Computation*, vol. 37 (155), 1981, pp. 141-158.
- [28] Coppoli, E. H. R., Mesquita, R. C., Silva, R. S., "Periodic boundary conditions in element free Galerkin method", *The International Journal for Computation and Mathematics in Electrical and Electronic Engineering*, vol. 28 (4), 2009, pp. 922-934.
- [29] Lu, Y. Y., Belytschko T., Gu L., "A new implementation of the element free Galerkin method", *Computer Methods in Applied Mechanics and Engineering*, vol. 113 (3-4), 1994, pp. 397-414.
- [30] Sibson, R., "A vector identity for the Dirichlet tessellation", *Mathematical Proceedings of the Cambridge Philosophical Society*, vol. 87 (1), 1980, pp. 151-155.
- [31] Yvonnet, J., *Mise en œuvre de la méthode des éléments naturels contrainte en 3D : application au cisailage adiabatique*, PhD dissertation, France : ENSAM Paris, 2008.
- [32] Takahashi, N., Ebihara, K., Yoshida, K., Nakata, T., Ohashi, K., Miyata, K., "Investigation of simulated annealing method and its application to optimal design of die mold for orientation of magnetic powder", *IEEE Transactions on Magnetics*, vol. 32 (3), 1996, pp. 1210-1213.
- [33] Colton, D., Kress, R., *Inverse Acoustic and Electromagnetic Scattering Theory*, Springer-Verlag, 1998.
- [34] Manzin, A., Bottauscio, O., "Element-Free Galerkin Method for the Analysis of Electromagnetic-Wave Scattering", *IEEE Transactions on Magnetics*, vol. 44 (6), 2008, pp. 1366-1369.
- [35] Wilcox, C. H., "An expansion theorem for electromagnetic fields", *Communications on Pure and Applied Mathematics*, vol. 9, 1956, pp. 115-134.
- [36] Lima, N.Z., Mesquita, R.C., Facco, W.G., Moura, A.S., Silva, E.J. "The Nonconforming Point Interpolation Method Applied to Electromagnetic Problems", *IEEE Transactions on Magnetics*, Vol 48 (6), 2012, pp. 619-622.

XI. Authors name and affiliation

Diego Pereira Botelho, Yves Marechal and Brahim Ramdane are from G2Elab, Grenoble University, CNRS, France.

Corresponding author:

Email: Yves.Marechal@Grenoble-inp.fr,

Phone: +33 4 76 82 71 36